



Original Manuscript

Peritoneal cavity-derived GATA6⁺ macrophages inhibit fibrosis through IL33 in endometrium

Lijie Yin^a, Jingman Li^a, Yue Dong^a, Jiali Wang^a, Xiuzhu Wang^a, Yajun Li^a, Yali Hu^{b,c}, Yayi Hou^{a,*}, Guangfeng Zhao^{b,c,**}

^a The State Key Laboratory of Pharmaceutical Biotechnology, Division of Immunology, Medical School, Nanjing University, Nanjing, China

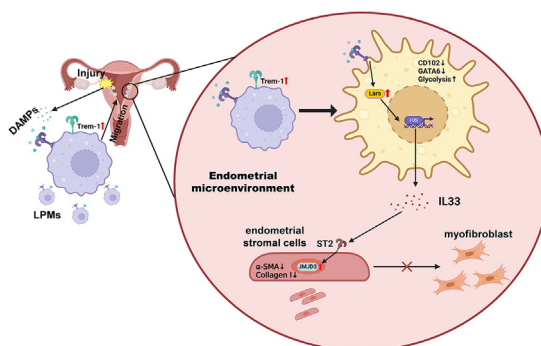
^b Department of Obstetrics and Gynecology, The Affiliated Nanjing Drum Tower Hospital of Nanjing University Medical School, Nanjing, China

^c Department of Obstetrics and Gynecology, Nanjing Drum Tower Hospital, State Key Laboratory of Pharmaceutical Biotechnology, Nanjing University, China

HIGHLIGHTS

- LPMs play a pivotal role in endometrial repair with LPMs-derived IL33 maintaining homeostasis and preventing fibrosis.
- DAMPs released by mechanically injured ESCs stimulate the migration of LPMs to the damaged uterus via Trem1.
- IL33 is upregulated in LPMs via the Lars-Fos axis enabling its binding to the enhancer region of the IL33 gene.
- LPMs-derived IL33 inhibits the differentiation of ESCs into myofibroblasts by binding to ST2 receptor on the surface of ESCs.
- IL33 upregulates the expression of JMJD3, which subsequently acts to suppress the fibrotic transformation of ESCs.

GRAPHICAL ABSTRACT



ARTICLE INFO

Article history:

Received 3 February 2025

Revised 10 June 2025

Accepted 28 June 2025

Available online 29 June 2025

Keywords:

Endometrial damage

Endometrial fibrosis

Large peritoneal macrophages

IL33

Endometrial repair

ABSTRACT

Macrophages exhibit a high degree of plasticity and play pivotal roles both in the normal physiological cycle of the endometrium and in its regeneration following injury. Although some new subsets of endometrial macrophages have been identified, their origins and functions remain to be further explored. In this study, we employed single-cell sequencing to analyze the endometrium of patients with normal endometrium and intrauterine adhesion (IUA) caused by injury. We identified a unique subset of macrophages distinguished by the expression of GATA6, a marker indicative of cavity macrophages. We verified that these GATA6⁺ macrophages were large peritoneal macrophages (LPMs) that migrated from the peritoneal cavity to the injured endometrium. Upon activation by injured endometrium, these LPMs demonstrated increased expression of Interleukin-33 (IL33), mediated by the Lars-Fos signaling axis, which interacts with the IL33 enhancer. Moreover, our studies revealed that IL33 derived from LPMs inhibited the differentiation of endometrial stromal cells (ESCs) into myofibroblasts, a critical step in the development of endometrial fibrosis. Furthermore, we confirmed the inhibitory effect occurred through the binding of IL33 to the ST2 receptor on ESCs, leading to the upregulation of JMJD3 and subsequent suppression

* Corresponding author.

** Corresponding author at: Department of Obstetrics and Gynecology, The Affiliated Nanjing Drum Tower Hospital of Nanjing University Medical School, Nanjing, China.

E-mail addresses: yayihou@nju.edu.cn (Y. Hou), zhaoguangfeng@nju.edu.cn (G. Zhao).

of myofibroblast differentiation. Our findings highlight the essential role of LPMs in promoting endometrial repair and inhibiting fibrosis in IUA.

© 2025 The Author(s). Published by Elsevier B.V. on behalf of Cairo University. This is an open access article under the CC BY-NC-ND license (<http://creativecommons.org/licenses/by-nc-nd/4.0/>).

Introduction

A healthy woman undergoes approximately 400 menstrual cycles over her lifetime. Under the regulation of hormonal fluctuations, the endometrium sequentially undergoes phases of proliferation, breakdown, and scarless repair. The underlying molecular and cellular mechanisms responsible for this scarless endometrial regeneration remain the focus of intensive research [1]. The human endometrium consists of two distinct layers: the basal layer and the functional layer. It is composed of various cell types, including epithelial cells, stromal fibroblasts, endothelial cells, immune cells, and stem cells [2]. During the process of physiological scarless repair of the endometrium, the controlled activation and regulation of immune cell responses play a pivotal role in orchestrating tissue regeneration [3]. Progesterone withdrawal stimulates endometrial stromal cells to release chemokines, attracting immune cells such as monocytes and macrophages into the endometrial tissue. Subsequently, these monocytes and macrophages rapidly differentiate into a pro-inflammatory phenotype, secreting matrix metalloproteinases (MMPs) to mediate extracellular matrix degradation and tissue breakdown. During the repair phase, these macrophages shift to a pro-reparative phenotype, contributing to tissue remodeling and regeneration [4].

Surgical trauma or severe infections can disrupt the endometrium's intrinsic repair process, leading to pathological fibrosis and the development of scar tissue. Intrauterine adhesions (IUA), also known as Asherman Syndrome, stand as a quintessential example of such endometrial fibrotic conditions. Patients with IUA often exhibit irregular menstruation, recurrent miscarriage, and infertility [5,6]. However, there is still no effective treatment available clinically. The transcervical resection of adhesions (TCRA), which is the preferred clinical approach, fails to fundamentally address the pathological changes of endometrial fibrosis, resulting in a high recurrence rate among IUA patients after surgery [7]. Therefore, understanding the pathophysiological mechanisms driving this condition is crucial to developing more effective and lasting therapeutic strategies.

Macrophages, characterized by their high plasticity, play a pivotal role in both the progression of endometrial repair and fibrosis. The modulation of M1 and M2 macrophage polarization is pivotal in influencing the pathogenesis and progression of IUA [8]. Our preliminary findings revealed a reduction in CD206⁺ M2 macrophages in the endometrium of patients with IUA [9]. Modulating macrophage polarization by increasing the M2/M1 ratio can suppress endometrial fibrosis and enhance pregnancy outcomes [10]. However, the M1/M2 classification of macrophages is now widely regarded as insufficient for accurately delineating the functional diversity and phenotypic heterogeneity of macrophages in specific biological contexts. Currently, an increasing number of novel macrophage subsets in the endometrium have been discovered to be involved in endometrial fibrosis. Our previous research found that CD301⁺ macrophages constitute a unique subset within the endometrial microenvironment. These macrophages facilitate the transdifferentiation of endometrial stromal cells (ESCs) into myofibroblasts, driving excessive extracellular matrix deposition and thereby playing a key role in the pathogenesis of endometrial fibrosis [11]. Additionally, we also discovered that IL34 can promote the differentiation of CX3CR1⁺ macrophages in the endometrium, thereby exacerbating the severity

of IUA [12]. Although there are few reports on tissue-resident macrophages in the endometrium, tissue-resident macrophages in other organs have shown distinct functional roles in the progression of fibrosis. For instance, during myocardial infarction, cardiac-resident macrophages respond to injury signals by initiating neutrophil recruitment and secreting beneficial immunoregulatory factors [13]. In spiny mice, tissue-resident macrophages promote auricular regeneration by secreting VEGFC and Lactotransferrin (LTF) [14]. These findings suggest that tissue-resident macrophages may play similarly pivotal roles in endometrial repair and fibrosis. This underscores the distinct roles played by different subsets of endometrial macrophages. Moreover, it is widely acknowledged that endometrial macrophages consist of both tissue-resident macrophages and macrophages or monocytes recruited from the periphery that differentiate locally, with each potentially exhibiting unique functions depending on their origin. GATA6⁺ macrophages within the peritoneal cavity, also known as large peritoneal macrophages (LPMs), have been reported to rapidly migrate to injured tissues such as the liver or intestine, where they play a reparative role [15,16]. However, their function in IUA remains unclear.

In this study, we hypothesize that a unique subset of peritoneal cavity-derived macrophages, characterized by GATA6 expression, plays a protective role in endometrial fibrosis following injury. Using 10x Genomics single-cell RNA sequencing (scRNA-seq), we identified these GATA6⁺ macrophages in the injured endometrium of IUA patients and confirmed that GATA6 and CD102 serve as defining markers of LPMs. We further propose that the depletion of LPMs exacerbates injury-induced endometrial inflammation and fibrosis in mice. Upon activation by the injured endometrium, LPMs upregulate Interleukin-33 (IL33), which, in turn, inhibits the differentiation of ESCs into myofibroblasts, thereby mitigating fibrosis via the ST2-JMJD3 signaling pathway. At the molecular level, we hypothesize that Lars enhances IL33 expression by promoting Fos binding to the IL33 enhancer. Collectively, our study aims to elucidate the functional role and regulatory mechanisms of LPMs in endometrial fibrosis and to explore the potential of LPM-derived IL33 as a therapeutic target for IUA.

Methods

Human samples

The human endometrial samples and procedures in this study were conducted with approval from the Ethics Committee of Nanjing Drum Tower Hospital (No. 2021-078-01). All participants provided written informed consent. Endometrial samples were obtained from women aged 22–40 years during the late proliferative phase of their menstrual cycle, collected during hysteroscopic examination. Samples were sourced from patients with IUA caused by dilation and curettage (D&C), whose endometrial condition scored above 8 according to the American Fertility Society's criteria, and from non-IUA patients who presented with tubal infertility, normal ovarian function, typical menstrual blood volume, and an endometrial thickness of at least 7 mm just before ovulation. Women were excluded from the study if they had any of the following conditions: positive serological results for HIV, hepatitis B or C, or syphilis; a history of tuberculosis; chronic endometritis; or vaginal bacterial or fungal infections. Addition-

ally, uterine malformations were ruled out via ultrasonography before sample collection.

Single-cell RNA-seq data processing

The methodology employed in this study is consistent with our previous report [11]. In brief, the endometrial samples were rinsed with PBS, cut into small pieces, and then digested with 0.1 % trypsin for 8 min, followed treatment with 0.8 mg/ml Collagenase Type I for 60 min at 37 °C with 5 % CO₂. The released cells were filtered, centrifuged, and treated with red blood cell lysis buffer before resuspension in PBS for single-cell 3' cDNA library preparation. Cells expressing fewer than 200 genes or with mitochondrial gene content >15 % were excluded. Single-cell encapsulation, cDNA library synthesis, and RNA sequencing were performed by Gene Denovo (Guangzhou, China). The data were aligned to the human genome (GRCh38) using the STAR algorithm, and the UMI count matrix was processed using the Seurat toolkit for normalization and log-transformation.

Cell culture

LPMs and ESCs were obtained from female Balb/C mice (8–10 Weeks) as previously described [17,18]. The peritoneal cavity of mice was lavaged with 5 mL of cool PBS for 2 min in a sterile environment. Isolated peritoneal cells were cultured in DMEM (Gibco, Grand Island, NY, USA) containing 10 % fetal bovine serum (FBS; Gibco, USA), 100 U/mL penicillin, and 100 µg/mL streptomycin (100 µg/mL; Gibco, Grand Island, NY, USA) and cultured at 37 °C with 5 % CO₂ and saturated humidity. After 4 h, the cells were rinsed 3 times with warm PBS to eliminate non-adherent cells, leaving only the adherent cells, which were identified as LPMs. In sterile environment, the uterus of mice was digested by mixture combine with DF-12 (Gibco, Grand Island, NY, USA), collagenase type I (Biosharp, CN), and DNase (Roche, Switzerland). Then 40 µM cell strainers were used to depart single-cells from uterus tissue. The ESCs were cultured in DF-12 containing 10 % fetal bovine serum (FBS; Gibco, USA), 100 U/mL penicillin, and 100 µg/mL streptomycin (100 µg/mL; Gibco, Grand Island, NY, USA) and cultured at 37 °C with 5 % CO₂ and saturated humidity. ESCs were used in P1–P3 in all experiments.

Animals and experimental protocol in vivo

Female Balb/C, C57BL/6 or CD45.1 mouse weighting 20–23 g (8–10 Weeks) were purchased from Nanjing Cavans Biotechnology Co, Ltd. They were housed in specific pathogen-free (SPF) condition with 12 h dark/light cycle, and could free access standard chow diets and water. All animal experiments were carried out in accordance with the guidelines of the Experimental Animals Management Committee (Jiangsu Province, China) and were approved by the Animal Protection and Ethics Committee of Nanjing University (IACUC-D2202077).

Electric tool-scratching mouse endometrial injury model

The electric tool-scratching mouse endometrial injury model was like the previous reported [19]. In brief, after anesthetizing the mice with isoflurane, the probe with a rough surface was insert into uterus and push the vibrator switch for 3-cycle (10 s shake and 2 s pause). This can cause mechanical damage to the endometrium. This method couldn't damage the integrity of the peritoneum, ensuring that there was no loss of LPMs. We detected the inflammation stage in 6 h after the model established, and the fibrosis stage in 7 Days after the model established.

LPMs depletion

After anesthetizing the mice with isoflurane, the mouse was lavage 2 times with PBS in a sterile environment. Endometrial injury model was established in mice after 24 h.

CD45.1⁺/CD45.2⁺ LPMs adoptive transfer

100µL clodronate liposomes (CLLs) were intraperitoneally injected into WT mice to deplete CD45.2⁺LPMs. After 48 h, CD45.1⁺LPMs were obtained from CD45.1 mouse and adoptive i. p. to WT mice. Endometrial injury model was established in mice after 24 h after successfully transfer [20].

Mechanical injury induces ESCs apoptosis

After the ESCs were affixed to the cell dishes for 24 h, they were forcefully detached from the dishes with DMEM complete medium and strongly blown up for 50 times. The supernatants were collected after 12 h of culturing the damaged ESCs and the mechanical damage-induced AES was obtained after filtration with a 0.22 µM filter.

Cell migration

LPMs were seeded in 3uM transwells, while apoptosis ESCs were seeded in the lower compartment of the transwells. The transwells were then put into 4 % PFA for 15 min in room temperature and subsequently washed 3 times with PBS. Following this, the transwells were placed in 1 % ammonium oxalate crystal violet for 45 min in room temperature and washed 3 times with PBS. Any LPMs that had not migrated to the opposite side were carefully removed using a cotton swab. The transwells were then placed under a microscope for observation. Three fields of view were randomly selected for cell counting, and the average value was counted.

RNA isolation and quantitative real-time PCR (qPCR)

Following the protocol of manufacturer, total RNA was extracted by Trizol reagent (Vazyme Biotech, China). Total RNA was reversed to cDNA by HiScript II Q RT SuperMix for qPCR (Catalogue # R222-01; Vazyme Biotech, China). The method of 2^{-ΔΔCT} was used to analysis the target genes expression levels, normalized by β-actin expression. The primers used in this study are listed in [Supplementary Table 1](#).

Western blot analysis (WB)

The protein of cells was lysed by RIPA lysis buffer (Beyotime Biotechnology) with protease inhibitor cocktail and phosphatase inhibitor cocktail (Roche), and clarified by centrifugation at 12,000g for 20 min. The BCA protein assay kit (Thermo) was used to determine the concentration of protein samples. Then protein samples were boiled in 99°C in Dry Bath Incubator, mixing 5X loading buffer. Protein samples were separated using SDS-PAGE, transferred to PVDF membranes and incubated in 5 % bovine serum albumin (BSA) in room temperature for 2 h. Primary antibody dilutions were added and incubated overnight at 4 °C in a shaker. The membrane was then incubated with secondary antibody coupled with HRP for 2 h at room temperature. Protein signals were observed using ECL solution and quantitative analysis of gray values was performed using Image J. The antibodies used in this study are listed in [Supplementary Table 2](#).

Gene silencing of *Lars*, *Trem1* and *Il33* using siRNA

Cells were transfected using Lipofectamine 3000 according to the manufacturer's guidelines (Invitrogen, USA). *Il33* small interfering RNA (siRNA) sequence (Si-*Il33*) was designed and purchased in Ribobio (Guangzhou, China). Si-*Lars* and si-*Trem1* were designed and purchased in Genescript (Shanghai, China). The sequences of siRNA are listed in [Supplementary Table 3](#).

Immunofluorescence

The cells were cultured in coverslip and subsequently fixed in 4 % paraformaldehyde (PFA) and wash 3 times using PBS. After permeabilization with 0.2 % Triton X-100, cells were incubated in 1 % BSA in room temperature for 1 h. Primary antibody dilutions were added and incubated overnight at 4 °C. After that, the cells were incubated with secondary antibody coupled with fluorescence for 2 h at room temperature in dark. The nuclei were stained by 4',6-diamidino-2-phenylindole (DAPI) and observed under FV3000 Laser Scanning Confocal Microscope (Olympus Corporation, Tokyo, Japan). Analyzing mean optical density or pearson's coefficient with image J. The antibodies used in this study are listed in [Supplementary Table 2](#).

Flow cytometry

The labeling of LPMs with fluorescent beads (Fluoresbrite® YG Microspheres, Polysciences Inc.) was performed using a method similar to that previously reported [21]. In brief, before establishing endometrial injury model in mouse, we injected a 100 uL mixture (10 uL fluo bead and 90uL PBS) to label the LPMs. Six hours after establishing endometrial injury model, we acquired the peritoneal lavage and uterine single-cell suspension. Fluorescent antibodies were used to label cells, and the antibodies used in this study are listed in [Supplementary Table 2](#). All flow cytometry data were acquired using the Beckman Coulter Cytoflex S (Beckman Coulter, CA, USA) or BD FACS Calibur cytometer (BD Biosciences, San Diego, CA, USA) and subsequently analyzed using FlowJo software (Treestar, Inc., San Carlos, CA, USA).

Immunohistochemistry

Paraffin blocks were sectioned into 2-μm-thick slices and mounted onto glass slides. To block endogenous peroxidase activity, the sections were treated with 3 % H₂O₂, and antigen retrieval was performed using Immunohistochemistry Universal Antigen Recovery Solution. The sections were then incubated overnight at 4 °C with diluted primary antibodies. Subsequently, they were incubated with HRP-conjugated secondary antibody, and the antigen signal was visualized with DAB. The sections were counterstained with hematoxylin, sealed with neutral resin, and the positive reactants were visualized under a microscope. The immunohistochemical staining was quantified by calculating the mean optical density using Image software. The antibodies used in this study are listed in [Supplementary Table 2](#).

Bulk RNA-sequencing and analysis

LPMs were treated with or without ASE for 6 h, and total RNA was extracted using Trizol reagent. RNA sequencing was performed on an Illumina NovaSeq 6000 platform by Hangzhou Astrocyte Technology Co., Ltd. (Hangzhou, China). Raw sequencing reads were processed using fastp to remove adapter sequences and low-quality reads. The clean reads were then mapped to the mouse reference genome (GRCm39) using HISAT2. Gene expression levels were quantified using featureCounts, and normalization was per-

formed using the Fragments Per Kilobase of transcript per Million mapped reads (FPKM) method. To account for potential batch effects, we applied the ComBat algorithm from the sva R package. Differential expression analysis between groups was conducted using DESeq2, with genes exhibiting a false discovery rate (FDR) below 0.05 and an absolute fold change (|FC|) ≥ 1.5 considered differentially expressed genes (DEGs). The quality of sequencing and mapping was assessed through principal component analysis (PCA) and sample clustering to ensure consistency across replicates.

Dual luciferase reporter assay

We selected a 2000 bp sequence upstream of the transcription start site (TSS) of the *Il33* gene (gene ID: 77125) as the promoter region (>NC_000085.7:29925060–29927060 Mus musculus strain C57BL/6J chromosome 19, GRCm39). The enhancer region for *Il33* was chosen from the NCBI database (>NC_000085.7:29922546–29923676 Mus musculus strain C57BL/6J chromosome 19, GRCm39). Corresponding luciferase reporter plasmids were constructed for both regions. Using the JASPAR database, we predicted the top three FOS::JUN binding sites and deleted these binding sites to generate the corresponding mutant plasmids.

Transfection was performed using Lipofectamine 3000 (Invitrogen), according to the manufacturer's protocol. For reporter assays, cells seeded in 24-well plates were transfected with 800 ng *Il33*-promoter-WT or *Il33*-promoter-MUT or *Il33*-enhancer-WT or *Il33*-enhancer-MUT, 800 ng Fos, and 100 ng Renilla plasmid. After 48 h, the cells were lysed, and reporter activity was measured using the Dual-Luciferase Reporter Assay System (Vazyme Biotech Co., Ltd.) following the manufacturer's instructions.

Statistical analysis

All the experiments were randomized and blinded, and each experiment was independently repeated at least three times. All values presented in the graphs are shown as means ± SEMs. The Shapiro-Wilk test was used to assess normality. For comparisons among more than two groups, one-way ANOVA was performed when data were normally distributed; for comparisons between two groups, unpaired Student's t-tests were used. Multiple testing corrections were applied to control for false positives: the false discovery rate (FDR) method was used for RNA-seq data, while Tukey's multiple comparisons test was employed for post hoc analysis following one-way ANOVA. If the data did not meet normality assumptions, non-parametric alternatives were applied. We have calculated and reported the effect sizes (Cohen's d for t-tests, and η² for one-way ANOVA) along with 95 % confidence intervals for all key group comparisons presented in the main figures. These are now summarized in a newly added [Supplementary Material 2](#). GraphPad Prism 5 Demo (GraphPad Software Inc., La Jolla, CA, USA) was utilized for statistical analysis.

Results

Result 1: GATA6⁺ macrophages in the injured endometrium are derived from the peritoneal cavity

By conducting 10x Genomic single-cell sequencing analysis on the endometrium samples collected from three healthy individuals and three patients with IUA, we discovered a distinct subpopulation of macrophages that express the cavity macrophage marker GATA6. This particular subpopulation is enriched in the endometrium of patients with IUA ([Fig. 1A](#) and [B](#), [Supplementary fig. 1A](#)). The immunostaining further showed that GATA6 was co-stained with macrophages marker CD68 in IUA endometria ([Fig. 1C](#)). Since

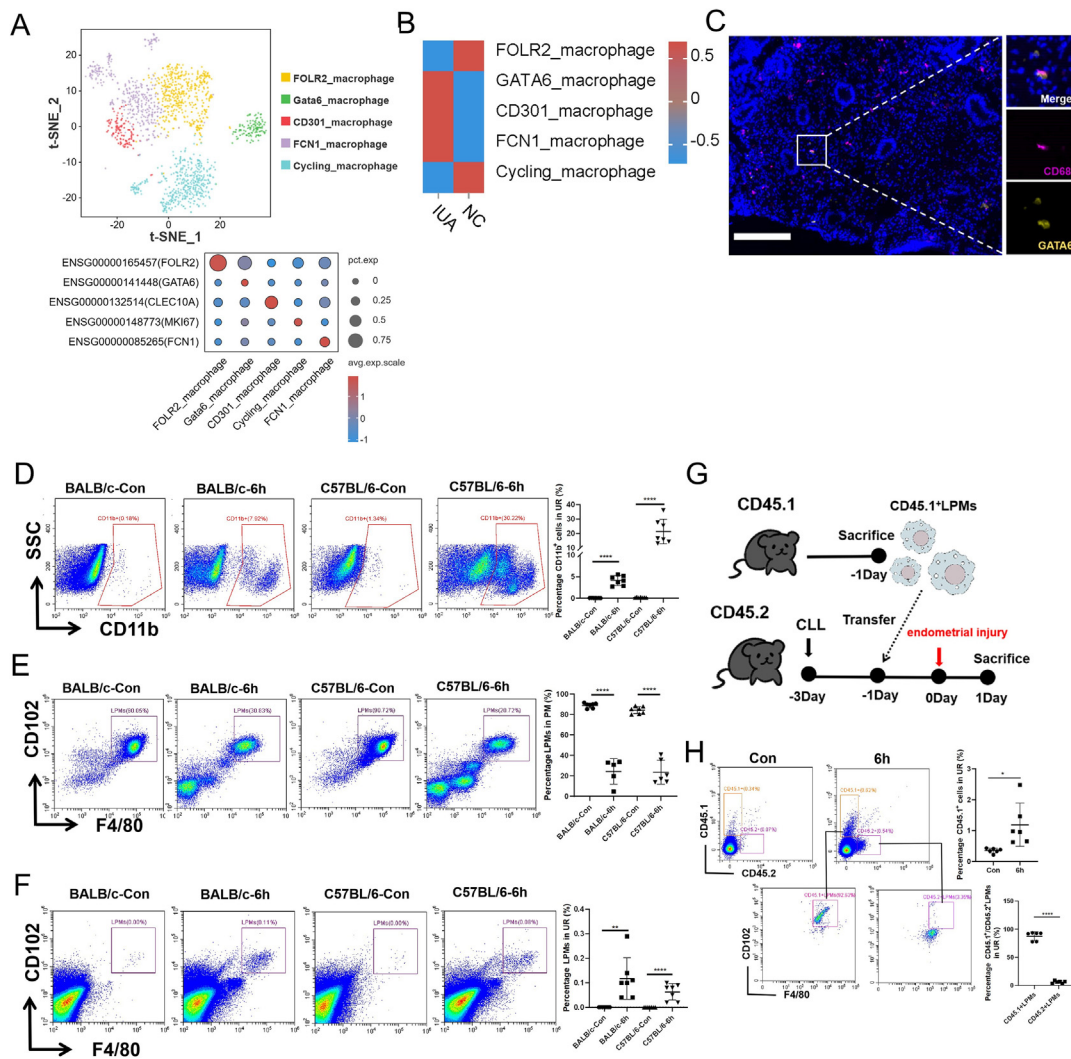


Fig. 1. GATA6⁺ macrophages (LPMs) in human or mouse endometrium between IUA patients and healthy controls. A. The tSNE plot displaying macrophages from normal control and patients with IUA (n = 3). B. Differences in macrophage subpopulations between normal control and patients. C. Representative immunofluorescence images of GATA6 and CD68 from samples of patients with IUA (Scale bar = 200 μm). D. Flow cytometry analysis of changes in the proportion of CD11b⁺ cells in the uterus of normal control and endometrial injury mice (n = 6). E. Flow cytometry analysis of changes in the proportion of LPMs in the peritoneal cavity of normal control and endometrial injury mice (n = 5–6). F. Flow cytometry analysis of changes in the proportion of LPMs in the uterus of normal control and endometrial injury mice (n = 6). G. Schematic diagram of the flow of CD45.1/CD45.2 adoptive transfer experiments. H. Flow cytometry analysis of changes in the proportion of CD45.1⁺ cells in the uterus of normal control and endometrial injury mice (n = 5–6). Values are mean ± SD. *p < 0.05, **p < 0.01, ***p < 0.001, ****p < 0.0001, ns denotes p > 0.05 (by unpaired Student's *t* test or one-way ANOVA).

the uterus is located in the peritoneal cavity, we hypothesize that this population of GATA6⁺ macrophages may originate from the peritoneal cavity. To validate this hypothesis, we established a mouse endometrial injury model. Six hours after inducing the injury, we collected peritoneal lavage fluid and uterine single-cell suspensions for flow cytometry analysis, following the gating strategy outlined in [Supplementary fig. 1B–C](#). The results revealed that endometrial injury triggered inflammation in the uterus, marked by a notable surge in the number of CD11b⁺ cells ([Fig. 1D](#)). Furthermore, there was a significant decline in LPMs in the peritoneal cavity ([Fig. 1E](#)) and a concomitant rise in LPMs in the uterus post-injury ([Fig. 1F](#)), indicating that LPMs may migrate from the peritoneal cavity to the injured uterus. To further confirm this phenomenon, we conducted CD45.1⁺/CD45.2⁺ LPMs adoptive transfer experiments [22] ([Fig. 1G](#)). The flow cytometry results showed that CD45.1⁺ cells were significantly reduced in the peritoneal cavity of Injured group (6 h group) compared to Control group ([Supplementary fig. 1D](#)). Conversely, the proportion of CD45.1⁺ cells was significantly elevated in the damaged uterus, and these CD45.1⁺ cells

were identified as F4/80⁺CD102⁺ cells (LPMs). Meanwhile, CD45.2⁺ cells in the damaged uterus were F4/80⁺CD102[−] cells ([Fig. 1H](#)). We did an isotype control of the flow-through antibody to rule out the possibility of a false-positive flow-through stain ([Supplementary fig. 1E](#)). These findings strongly indicated that LPMs migrate from the peritoneal cavity to the damaged uterus both in human and mouse.

Result 2: depletion of LPMs exacerbates inflammation and fibrosis within the injured endometrium

To investigate the role of LPMs in damaged endometrium, we initially employed intraperitoneal lavage (PL) to specifically remove LPMs from the peritoneal cavity. The results showed that PL did not elicit a systemic inflammatory response or uterine damage in mice ([Supplementary fig. 2A, B, C](#)). Flow cytometry analysis further confirmed that PL effectively and stably depleted LPMs in the peritoneal cavity of mice, not SPMs ([Fig. 2A, Supplementary fig. 2D](#)). After establishing the endometrial injury model, we

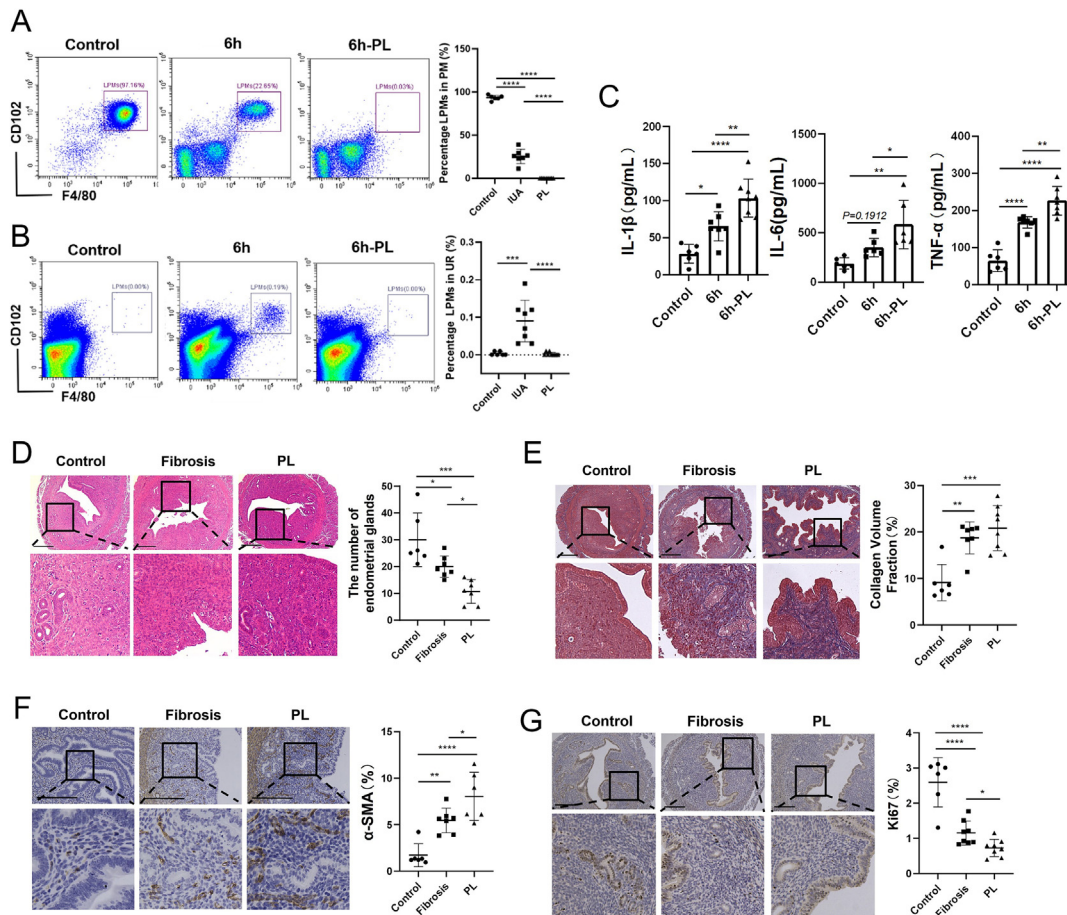


Fig. 2. Depletion of LPMs exacerbates inflammation levels and endometrial fibrosis in endometrial injury mice. A. Flow cytometry analysis of changes in the proportion of LPMs in the peritoneal cavity ($n = 6-8$). PL means depleting LPMs by intraperitoneal lavage. B. Flow cytometry analysis of changes in the proportion of LPMs in the uterus ($n = 6-8$). C. Serum concentrations of IL-1 β , IL-6, and TNF- α were measured by ELISA ($n = 6$). D. HE staining of endometrial tissues obtained from mice ($n = 6-7$, Scale bar = 200 μm). E. Masson's trichrome staining of endometrial tissues obtained from mice ($n = 6-7$, Scale bar = 200 μm). F. Representative images of IHC for α -SMA staining in the mice endometria ($n = 6-7$, Scale bar = 200 μm). G. Representative images of IHC for Ki67 staining in the mice endometria ($n = 6-8$, Scale bar = 200 μm). Values are mean \pm SD. * $p < 0.05$, ** $p < 0.01$, *** $p < 0.001$, **** $p < 0.0001$ ns denotes $p > 0.05$ (by one-way ANOVA).

observed a notable absence of significant LPMs cluster in the damaged uterus of the PL group (Fig. 2B), suggesting that LPMs depletion prevented their migration to the injured uterus. Our results also demonstrated that the injury significantly elevated the systemic inflammation level in mice, as evidenced by the marked upregulation of serum inflammatory factors IL-1 β , IL-6, and TNF- α . This inflammatory response was further exacerbated by the depletion of LPMs (Fig. 2C). Additionally, following endometrial injury, we observed a significant reduction in the number of endometrial glands, an increase in collagen deposition, an upregulation of the fibrosis marker α -SMA, and a decrease in the expression of the cell proliferation marker Ki67. Depletion of LPMs exacerbated these injury and fibrotic symptoms (Fig. 2D-G). The compensatory infiltration of CD86 $^{+}$ and CD301 $^{+}$ macrophages upon LPMs depletion highlights the complexity of macrophage network interactions during endometrial repair (Supplementary fig. 2 D, E). Taken together, these data suggested that LPMs migrating into damaged endometrium might play a protective role, promoting the repair of endometrial injury.

Result 3: the LPMs entering the damaged endometrium undergoes phenotypic changes

We utilized fluorescent beads to track LPMs (Beads $^{+}$ LPMs). These beads specifically labeled LPMs with a 91 % efficiency (Sup-

plementary fig. 3A) and did not stain the undamaged uterus with fluorescence from the beads (FITC) (Supplementary fig. 3B). We then collected peritoneal lavage and uterine single-cell suspensions at 0, 6, 12, 24, and 48 h after establishing the endometrial injury model, and analyzed these samples using flow cytometry. The results revealed that Beads $^{+}$ LPMs persistently migrated into the damaged uterus within 48 h, accompanied by a decrease in the LPMs marker CD102 (Fig. 3A). We further confirmed the labeling of LPMs by immunofluorescence co-localization, which showed that Beads $^{+}$ CD102 co-localized at 6 and 12 h (Fig. 3B). Additionally, there was no co-localization of Bead fluorescence and TUNEL fluorescence at 24 and 48 h, indicating that the labeled LPMs did not undergo apoptosis at these time points (Fig. 3C). These findings indicated that the observed CD102 reduction within Beads $^{+}$ cells were reflective of alterations in LPMs specifically, rather than changes in other macrophage populations present in the uterus. The Beads $^{+}$ CD11b $^{+}$ cells in the peritoneal cavity exhibited a similar trend of change as LPMs, further validating the success of our LPMs labeling (Supplementary fig. 3 C, D). We also observed that LPMs could penetrate the uterine muscle layer and accumulate at the damaged endometrium, indicating that LPMs alleviate endometrial fibrosis by interacting with cells at the endometrial site (Fig. 3D).

Endometrial injury can result in some cell death of stromal cells in uteri. Therefore, we established a method to induce the death of endometrial stromal cells (ESCs) through mechanical force (Sup-

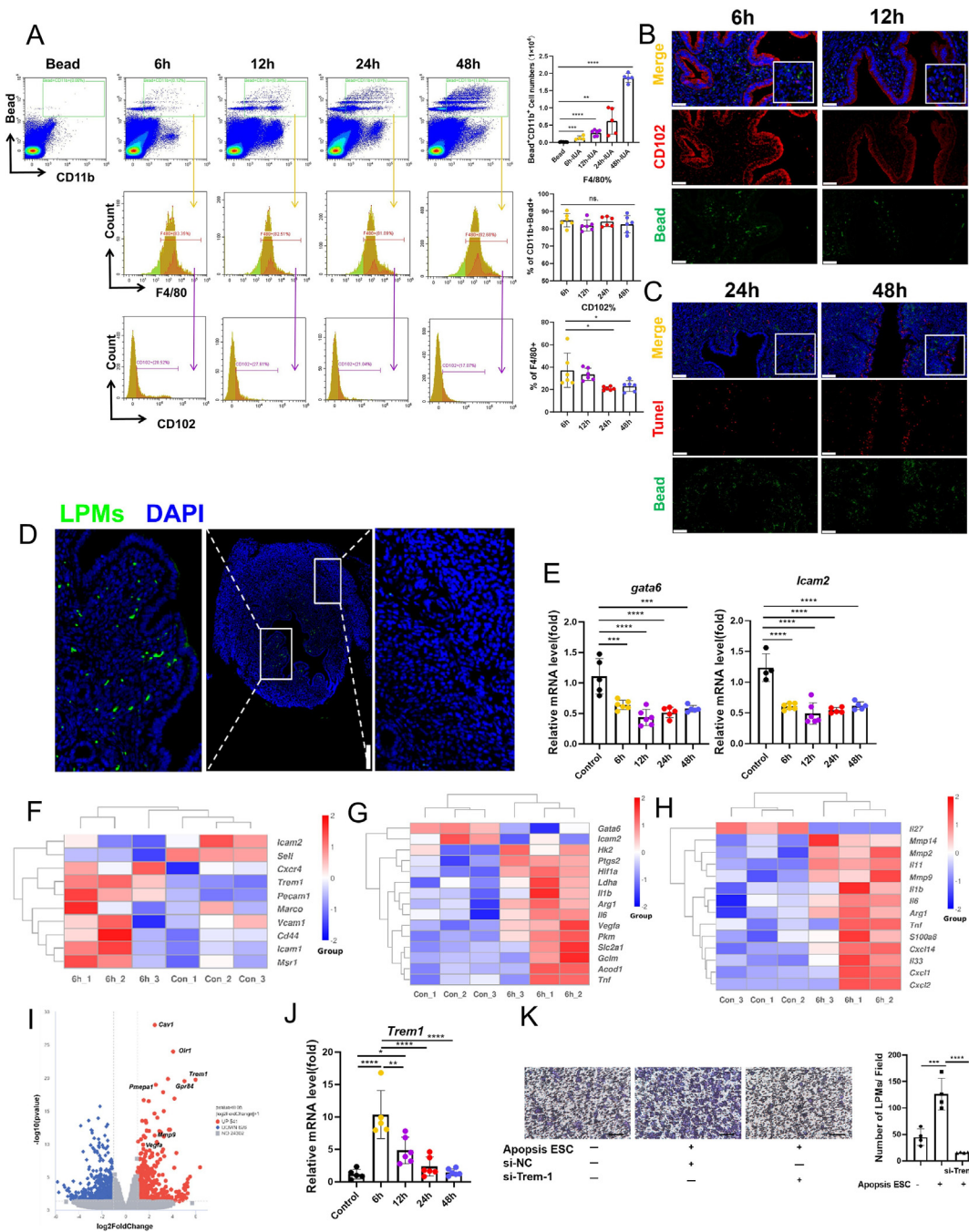


Fig. 3. LPMs responding to wound signaling change their transcriptome profile. **A**. Flow cytometry analysis of changes in the proportion of Beads⁺LPMs and the change of them in the mice uterus (n = 5–6). **B**. Representative images of immunofluorescence for CD102 and Bead in the endometrial injury mouse endometria (Scale bar = 50 μ m). **C**. Representative images of immunofluorescence for tunel and Bead in the endometrial injury mouse endometria (Scale bar = 100 μ m). **D**. Representative images of immunofluorescence for Bead in the endometrial injury mouse uterus (Scale bar = 200 μ m). **E**. The gene levels of *Gata6* and *Icam2* were detected with qRT-PCR (n = 5–6). **F**. The thermogram of migration-associated molecule related genes expression pattern. **G**. The thermogram of early-phase wound macrophages and LPMs phenotype related genes expression pattern. **H**. The thermogram of cytokines related genes expression pattern. **I**. The volcano figure showed foldchanges of genes in LPMs incubated with control or AES-treated LPMs (6 h). **J**. The gene levels of *Trem1* were detected with qRT-PCR (n = 5–6). **K**. Crystal violet staining of LPMs cocultured with apoptosis ESCs or not (Scale bar = 100 μ m). Values are mean \pm SD. *p < 0.05, **p < 0.01, ***p < 0.001, ****p < 0.0001, ns denotes p > 0.05 (by unpaired Student's *t* test or one-way ANOVA). (For interpretation of the references to colour in this figure legend, the reader is referred to the web version of this article.)

plementary fig. 4 A). Subsequently, we treated LPMs with the apoptotic ESCs supernatant (AES). Consistent with in vivo findings, the LPMs markers *Gata6* and *Icam2* (encoding CD102) exhibited significant downregulation starting from 6 h (Fig. 3E). We also subjected LPMs to AES for 0 or 6 h for comprehensive genome-wide mRNA expression analysis. Principal Component Analysis (PCA) of the samples revealed distinct clustered distributions between

the two groups, which could be clearly separated into two sample clusters (Supplementary fig. 4B). Compared to the control group, a total of 1,187 differentially expressed genes (DEGs) were identified in the LPMs treated with AES for 6 h, with 541 genes up-regulated and 646 genes down-regulated (Fig. 3I). Heatmaps of DEGs indicated that gene expression patterns clustered distinctly after unsupervised clustering (Supplementary fig. 4C). Migration-associated

molecules (Fig. 3F), early-phase wound macrophage-associated molecules and phenotypic markers of LPMs (Fig. 3G; Supplementary fig. 4D), and cytokines (Fig. 3H) displayed different transcriptomic profiles, suggesting alterations in AES-activated LPMs compared to their resting state. The volcano plot of differential genes highlighted that Triggering receptor expressed on myeloid cells 1 (*Trem1*) was significantly overexpressed at 6 h (Fig. 3I). *Trem1*, a cell surface receptor found on monocytes or tissue-resident macrophages, can be activated by damage-associated molecular patterns (DAMPs) and is transcriptionally regulated by *Hif1 α* [23]. The qRT-PCR results verified that *Trem1* expression was significantly high at 6 h, followed by a decline and a gradual return to baseline levels (Fig. 3J). *Trem1* is known to promote macrophages migration and adhesion [24]. Expectedly, Results from the transwell migration assay indicated that AES treatment enhanced LPMs migration, while knockdown of *Trem1* inhibited this migration process (Fig. 3K). These findings implied that DAMPs released from the damaged endometrium may promote LPMs migration by upregulating *Trem1* expression. These findings implied that DAMPs released from the damaged endometrium may promote LPMs migration by upregulating *Trem1* expression. What's interesting was that the DAMPs could also change the LPMs phenotype. However, phenotypic changes in LPMs related to their functional alterations and the repair of the injured endometrium remains unclear.

Result 4: changed LPMs phenotypically secrete IL33 to promote endometrial repair

To further determine the proteins integral to macrophages functionality secreted by activated LPMs, the gene expressions of secretory proteins transcriptomic profiles (Fig. 3H) were investigated by qRT-PCR. Notably, *IL33* and *Arg1* were significantly upregulated in LPMs within the 6 h group (Supplementary Fig. 5A). ScRNA-seq analysis also revealed the specific and high expression of *IL33* in LPMs (Fig. 4A), with co-localization of *IL33* and *Gata6* evident (Fig. 4B; Supplementary Fig. 5B). Importantly, we identified CD68⁺GATA6⁺IL33⁺ macrophages in the endometrium of IUA patients (Fig. 4C). At 6 h of AES treatment, LPMs exhibited peak *IL33* gene expression (Fig. 4D), with *IL33* protein levels reaching their maximum at 12 h (Fig. 4E; Supplementary Fig. 5C), suggesting that DAMPs released from injured ESCs may activate LPMs, leading to the upregulation of *IL33*. To confirm our hypothesis, we treated LPMs with ATP, a classical DAMPs. The results showed that ATP promoted *IL33* expression at both the gene and protein levels (Supplementary Fig. 5 D, E, F). Concurrently, AES treatment significantly upregulated Ki67 expression in LPMs (Fig. 4F, G). A marked increase in the proportion of CD11b⁺F4/80⁺IL33⁺ cells was also observed during the progression of endometrial injury in vivo (Fig. 4H). Altogether, damaged endometrial tissue can activate LPMs, resulting in the robust expression of *IL33*.

To determine whether the inhibitory effect of LPMs on endometrial fibrosis is mediated through the secretion of *IL33*, we directly treated the endometrial injury mouse model with *IL33* recombinant protein. Following the intraperitoneal administration of 0.25 μ g, 0.5 μ g, or 1 μ g of *IL33* recombinant protein, we evaluated the condition of mice with endometrial injury (Fig. 4I). The results showed that intraperitoneal injection of *IL33* inhibited effectively both uterine inflammation and systemic inflammation induced by endometrial injury (Supplementary fig. 5G, Fig. 4J). Additionally, it triggered a type 2 immune response that facilitated tissue repair (Supplementary fig. 5H). Importantly, this treatment did not increase serum levels of *IL33* and sST2, a specific soluble receptor for *IL33* (Supplementary fig. 5I). *IL33* was found to preserve the normal morphology and quantity of uterine glands (Fig. 4K), inhibit collagen deposition (Fig. 4L) and α -SMA expression in the endome-

trium (Fig. 4M), and enhance CD31 expression (Fig. 4N). These results suggested that intraperitoneal injection of *IL33* can alleviate injury induced endometrial fibrosis.

Furthermore, we collected endometrial tissue samples from patients with IUA of varying degrees of clinical severity. Our analysis revealed a notable trend: the Pearson's correlation coefficient between CD68 and *IL33* was higher in patients with mild disease, and this correlation progressively diminished as the severity of the disease increased. Consistent with this finding, the fluorescence intensity of *IL33* was also observed to be higher in patients with less severe disease, decreasing as the disease severity escalated (Fig. 4O). In brief, LPMs migrated to the damaged endometrium and secreted *IL33* to promote uterine repair and inhibit endometrial fibrosis.

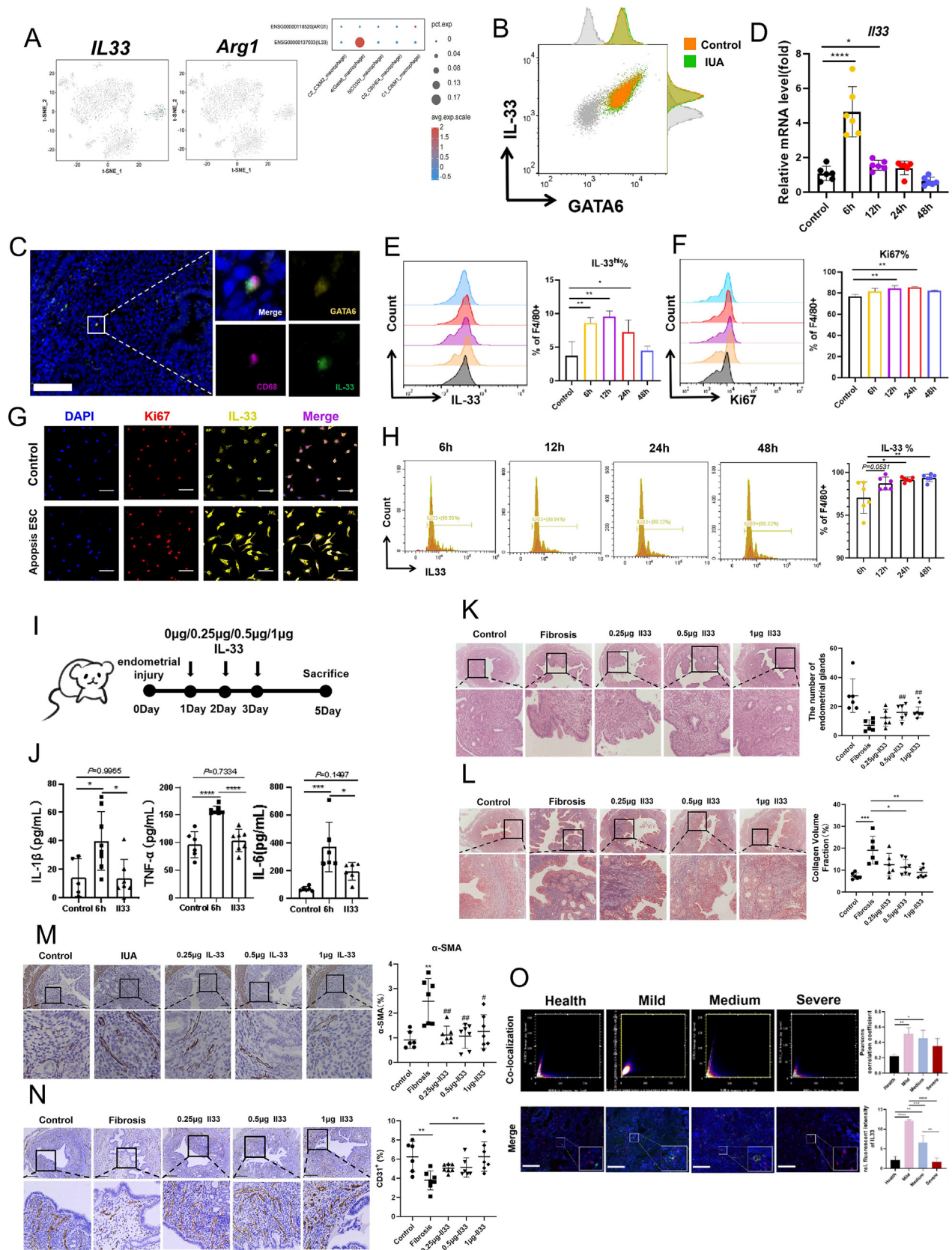
Result 5: *IL33* inhibits the differentiation of ESCs into myofibroblasts by upregulating JMJD3 via ST2

ST2 is the sole receptor for *IL33* signaling. Our observations revealed a notable upregulation of ST2 expression in the uterine tissues of mice with endometrial injury, with specific localization on ESCs (Fig. 5A, B). A key factor in the development of endometrial fibrosis is the accumulation of myofibroblasts, with the transdifferentiation of endometrial stromal cells (ESCs) into myofibroblasts [11,25]. We induced ESCs differentiation toward myofibroblasts using TGF- β 1 and subsequently co-cultured them with non-activated LPMs, activated LPMs, activated LPMs with *IL33*-knockdown, or recombinant *IL33* (Fig. 5C). The results showed that TGF- β 1 led to a significant increase in α -SMA expression in ESCs, which was not substantially affected by non-activated LPMs. However, activated LPMs inhibited α -SMA expression, and this suppressive effect was abrogated when *IL33* was knocked down in the activated LPMs. Additionally, activated LPMs suppressed the gene expression of *Acta2* (encoding α -SMA) and *Col1a1* (encoding Collagen I), but this inhibition was reversed when *IL33* was knocked down prior to LPMs activation (Fig. 5D). Similar results were obtained upon the addition of recombinant *IL33* protein (Supplementary Fig. 6 A, B, C). Furthermore, our findings revealed that activated LPMs elevated both the mRNA and protein levels of *Kdm6b* (encoding JMJD3) in ESCs, and this increase was reversed when *IL33* was knocked down (Fig. 5E, F). Prior research has shown that JMJD3 in renal interstitial cells exhibits anti-fibrotic effects by limiting multiple pro-fibrotic signaling pathways [26]. These results indicate that *IL33* inhibits TGF- β 1-induced fibrosis by upregulating JMJD3 expression in ESCs.

Given that ST2 is highly expressed in the uterine tissues of mice with endometrial injury, we hypothesized that *IL33* might regulate the differentiation of ESCs into myofibroblasts via ST2 on ESCs. To validate this hypothesis, we used sST2 to block *IL33* from binding to ST2 on ESCs during differentiation induction with TGF- β 1. Our results demonstrated that the addition of sST2 reversed the inhibitory effects of activated LPMs on α -SMA protein expression (Fig. 5G) and downregulated the gene expression of *Acta2*, *Col1a1*, and *Kdm6b* (Fig. 5H). These findings indicated that activated LPMs inhibited the differentiation of ESCs into myofibroblasts by secreting *IL33*, which exerts its effects via the ST2- JMJD3 axis in ESCs.

Result 6: *Lars-Fos* axis drives the *IL33* expression of LPMs by binding to its enhancer

Given the elevated expression of *IL33* in activated LPMs and its pivotal role in inhibiting inflammation and endometrial fibrosis, we sought to elucidate the molecular mechanisms driving *IL33* expression. To this end, we conducted a functional enrichment analysis of DEGs using the Kyoto Encyclopedia of Genes and Genomes (KEGG) pathway (<https://www.kegg.jp/>). Our analysis



revealed significant enrichment in pathways related to aminoacyl-tRNA ligase activity, cell adhesion molecule binding, and the aminoacyl-tRNA synthetase multienzyme complex (Fig. 6A). Gene Ontology (GO) analysis (<https://geneontology.org/>) indicated that DEGs upregulated at 6 h post-AES treatment were mainly enriched in the Pentose Phosphate Pathway, HIF-1 signaling pathway, and Aminoacyl-tRNA biosynthesis (Fig. 6B). Gene Set Enrichment Analysis (GSEA) (<https://www.gsea-msigdb.org/gsea/msigdb>) also showed that upregulated genes were significantly associated with aminoacyl-tRNA ligase activity (Fig. 6C). Collectively, these results established a link between DEGs in the 6-hour group and aminoacyl-tRNA activity. A heatmap analysis of this pathway pinpointed leucyl-tRNA synthetase (Lars) as being notably upregulated at 6 h (Fig. 6D). Since Lars mediates the activation of the mechanistic target of rapamycin complex 1 (mTORC1) [27], we speculated that AES might regulate IL33 expression via Lars, as their expression patterns were closely aligned (Fig. 6E).

To explore the intricate molecular mechanisms, we utilized the ChEA3 database (<https://maayanlab.cloud/chea3/>) to identify the top 10 transcription factors (TFs) linked to upregulated DEGs in LPMs after 6 h of AES treatment. Among these, Fos stood out as a pivotal TF, engaging in interactions with the remaining nine TFs (Fig. 6F). As the Fos family forms a tight complex with the Jun family to constitute the major component of AP-1, we integrated expression of Fos and Jun family members in our RNA-seq data and found the Fos was the significant expression gene in them (Supplementary Fig. 7A), a result further validated by qRT-PCR (Fig. 6G). Additionally, by using the STRING database (<https://cn.string-db.org/>), we also identified a robust correlation between Fos and Lars (Fig. 6H), prompting us to postulate that Lars regulates Fos expression. Knockdown of *Lars* via siRNA resulted in a concomitant decrease in Fos gene expression (Fig. 6I). Moreover, either knocking down *Lars* or inhibiting Fos's DNA-binding activity with T-5224 significantly reduced IL33 expression at both transcriptional and protein levels (Fig. 6J, K). These findings suggest that in LPMs, Lars modulates IL33 gene expression by regulating Fos.

Fos typically promotes gene expression by binding to promoters or enhancers [28,29]. Using the enhancer and promoter regions of IL33 predicted by NCBI (<https://www.ncbi.nlm.nih.gov/gene/>), we conducted an analysis of these sequences within the UCSC Genome Browser (<https://genome.ucsc.edu/>) and identified potential binding sites for Fos. Further motif prediction using the JASPAR database (<https://jaspar.elixir.no/>) confirmed these findings (Supplementary Fig. 7B, C). Dual-luciferase reporter assays demonstrated that the transfection of Fos significantly enhanced luciferase activity driven by the IL33 enhancer region, and this effect was abolished when Fos-binding motifs were mutated (Fig. 6L–M). ChIP-PCR analysis further confirmed that FOS directly binds to the predicted enhancer regions of the IL33 gene (Supplementary Fig. 7D). This phenomenon was not observed in the promoter of IL33. Collectively, these results indicated that AES upregulates Lars, which subsequently enhances Fos binding to the IL33 enhancer, thus promoting IL33 expression in LPMs.

Discussion

In this study, we identified a unique subset of macrophages, termed GATA6⁺ macrophages or LPMs, that originally reside in the peritoneal cavity but subsequently migrate to the injured endometrium. Upon activation by injured endometrium, these LPMs exert an inhibitory effect on endometrial fibrosis by secreting IL33. Mechanistically, the upregulation of IL33 expression in activated LPMs is orchestrated by the Lars-Fos signaling axis, which binds to the enhancer region of the IL33 gene. IL33, produced by LPMs, suppresses the differentiation of ESCs into myofibroblasts by activating the ST2-JMJD3 signaling pathway in ESCs, thereby attenuating the fibrotic response in the endometrium.

GATA6⁺ macrophages, also referred to as LPMs in the peritoneal cavity, represent a subpopulation of macrophages that reside within the peritoneal, pleural, and pericardial cavities [3]. In their basal state, LPMs demonstrate swift mobility within the peritoneal cavity, partly attributed to diaphragmatic motion during respiration. However, in response to tissue or organ damage, LPMs are quickly recruited to the injury site, accumulate there within minutes [30]. For instance, following liver [16] or gut [15] injuries, LPMs migrate from the peritoneal cavity to the damaged region, initiating repair processes that promote revascularization and tissue regeneration. Similarly, GATA6⁺-pericardial cavity macrophages (GPCMs) play a crucial role in cardiac repair and revascularization following myocardial infarction. Studies have shown that upon migration to the damaged heart, GPCMs experience a downregulation in GATA6 and CD102 expression without impairing their anti-fibrotic functions. However, the possibility of false-positive results in this context cannot be entirely excluded by the authors [21]. Our previous research demonstrated that mesenchymal stem cells (MSCs) facilitate the migration of LPMs to the injured endometrium, where LPMs phagocytose ferroptotic macrophages at the injury site, thereby providing protective effects to the injured uterus [18]. However, the functional roles of LPMs following their migration to the damaged endometrium, as well as the precise mechanisms underlying these effects, remain largely unknown. In this study, through the analysis of clinical samples and murine experiments, we further characterized the migration of LPMs from the peritoneal cavity to the uterus during endometrial injury. Depletion of LPMs exacerbated the severity of the disease. By using fluorescent beads for the specific labeling of LPMs, we eliminated the possibility of false-positive results and observed phenotypic changes in LPMs after their migration to the damaged endometrium. Although our findings indicate the presence of LPMs within the endometrium following injury, we cannot yet conclusively determine whether these cells traverse the uterine myometrium or are indirectly represented via surface adhesion and phagocytosis-based mechanisms. Future studies using genetically fate-mapped LPMs are warranted to trace their precise localization and migratory dynamics in the context of uterine injury. RNA-seq revealed that

Fig. 4. Activated LPMs highly express IL33 to relieves endometrial injury. A. The tSNE plot showing the expression of IL33 and Arg1 for macrophages. B. Flow cytometry analysis of GATA6 and IL33 in LPMs. C. Representative immunostaining images of CD68, GATA6 and IL33 from samples of IUA patients (Scale bar = 100 μ m). D. The gene levels of IL33 was detected with qRT-PCR (n = 6). E. Flow cytometry analysis of IL33 in AES treated LPMs (n = 4). F. Flow cytometry analysis of Ki67 in AES treated LPMs (n = 4). G. Representative immunofluorescence images of IL33 and Ki67 from samples of LPMs (Scale bar = 40 μ m). H. Flow cytometry analysis of changes in the proportion of Bead⁺CD11b⁺IL33⁺ cells in the endometrial injury mice uterus (n = 5–6). I. Schematic diagram of the procession of endometrial injury model. J. Serum concentrations of IL-1 β , TNF- α , and IL-6 were measured by ELISA (n = 7). K. HE staining of endometrial tissues obtained from mice (n = 7). L. Masson's trichrome staining of endometrial tissues obtained from mice (n = 7). M. Representative images of IHC for α -SMA staining in the mice endometria (n = 7, Scale bar = 200 μ m). N. Representative images of IHC for CD31 staining in the mice endometria (n = 7, Scale bar = 200 μ m). O. Representative immunofluorescence images of IL33 and CD68 from samples of patients with IUA (n = 3–5, Scale bar = 200 μ m). Values are mean \pm SD. *p < 0.05, **p < 0.01, ***p < 0.001, ****p < 0.0001, ns denotes p > 0.05 (by unpaired Student's t test or one-way ANOVA).

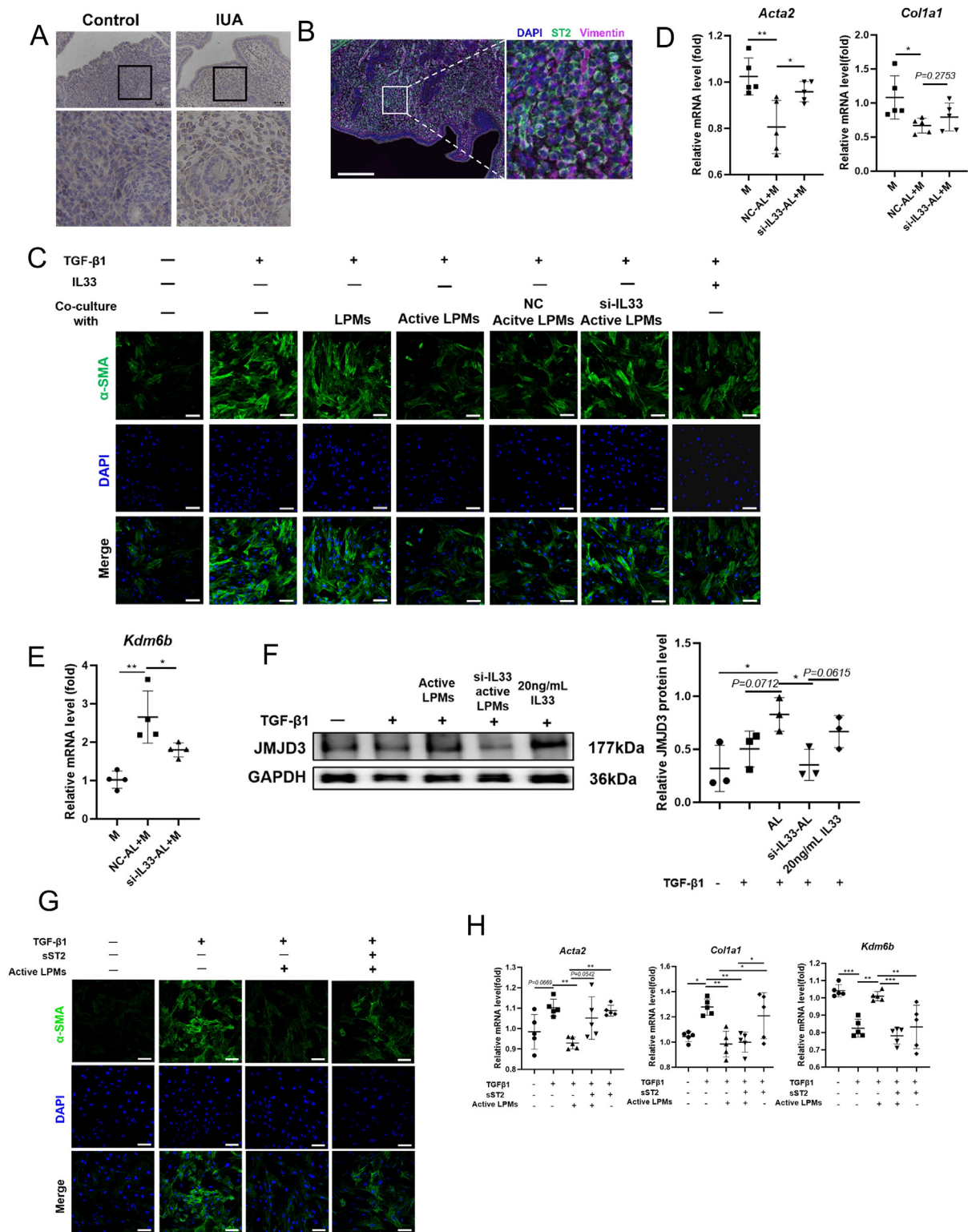
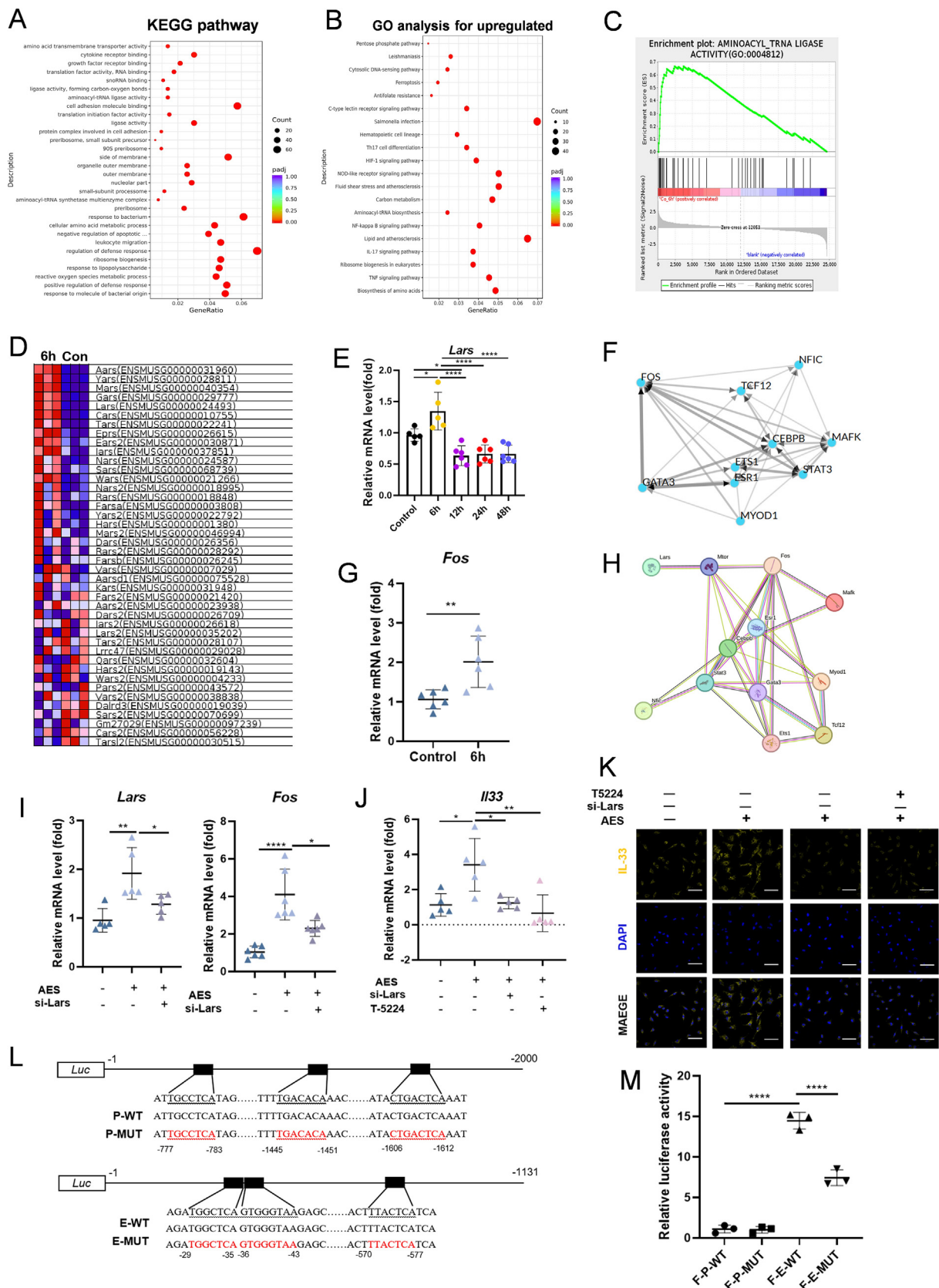


Fig. 5. LPMs-derived IL33 inhibits differentiation of ESCs into myofibroblasts via JMJD3. A. Representative images of IHC for ST2 staining in the mice endometria (n = 3, Scale bar = 100 μ m). B. Representative images of immunofluorescence for ST2 and Vimentin in the endometrial injury mouse endometria (n = 3, Scale bar = 200 μ m). C. Representative immunofluorescence images of α -SMA from samples of ESCs (n = 3, Scale bar = 100 μ m). (with or without TGF β 1(10 ng/mL), with or without IL33 (20 ng/mL), with or without active-LPMs/ LPMs in resting). D. The gene levels of *Acta2* and *Col1a1* were detected with qRT-PCR (n = 5). E. The gene levels of *Kdm6b* were detected with qRT-PCR (n = 4). F. The protein levels of *Jmjd3* were detected with WB (n = 3). G. Representative immunofluorescence images of α -SMA from samples of ESCs (n = 3) (scale bar: 100 μ m). H. The gene levels of *Acta2*, *Col1a1* and *Kdm6b* were detected with qRT-PCR (n = 5). Values are mean \pm SD. *p < 0.05, **p < 0.01, ***p < 0.001, ****p < 0.0001, ns denotes p > 0.05 (by unpaired Student's t test or one-way ANOVA).



activated LPMs displayed distinct transcriptional profiles, indicating a reprogramming of these cells upon activation, consistent with previous reports [16,21].

The role of IL33 in fibrosis continues to be an area of intense research. IL33 recombinant protein therapy at doses ranging from 0.4 µg to 1 µg, has demonstrated efficacy in alleviating fibrosis in multiple organs, including the heart [31], kidneys [32], and colon [33], as well as promoting tissue repair in skin wounds [34,35]. However, Liu et al. reported that intrauterine injection of a higher dose of IL33 (4 µg) exacerbated IUA [36]. This dose notably exceeds the therapeutic range for anti-fibrotic effects and the serum levels typically associated with disease pathology. In fact, doses within this higher range have been associated with the promotion of fibrosis [37,38]. These observations imply a dose-dependent effect of IL33 on fibrosis, with lower doses inhibiting fibrosis and promoting tissue repair, while higher doses may exacerbate it. In our study, intraperitoneal administration of IL33 at doses ranging from 0.25 µg to 1 µg effectively mitigated systemic inflammation and reduced endometrial fibrosis in a mouse model of endometrial injury. Furthermore, in clinical endometria with varying severities of IUA, we observed an upregulation of IL33 expression in GATA6⁺ macrophages, which diminished as disease severity increased. This suggests that IL33 levels secreted by LPMs are inversely correlated with the severity of IUA, further supporting the hypothesis that low doses of IL33 secreted by LPMs inhibit endometrial fibrosis.

However, our results do not suggest that simply replacing LPMs with low-dose recombinant IL33 injection represents the optimal therapeutic strategy for endometrial fibrosis. Although exogenous IL33 administration can be achieved through injections or drug delivery systems, LPMs may be essential for modulating the local IL33 microenvironment and fine-tuning its release. The direct application of IL33 poses challenges in precise dose regulation and may increase the risk of adverse effects, whereas IL33 secretion by LPMs could provide a more physiologically regulated approach to maintaining therapeutic levels. Furthermore, LPMs may play broader roles in tissue repair beyond IL33 secretion, potentially facilitating interactions with other immune cells and supporting additional regenerative processes [18,39]. A compromised ability of LPMs to produce IL33, possibly due to underlying pathological conditions or immune dysfunction, could contribute to the pathogenesis in some patients. Investigating the molecular mechanisms governing IL33 secretion by LPMs could help identify patient subgroups who are most likely to benefit from IL33-based therapies or guide the development of personalized treatment regimens tailored to individual immune profiles.

The differentiation of ESCs into myofibroblasts is a critical step in endometrial fibrosis progression. Previous research has shown that inhibition of JMJD3 enhances TGFβ1 signaling in renal mesangial cells, thereby promoting their transition into myofibroblasts [26]. Our findings indicated that IL33 inhibits the differentiation of ESCs into myofibroblasts by binding to its receptor ST2, which subsequently upregulates JMJD3 expression in ESCs. Given that

JMJD3 has been reported to suppress TGF-β signaling, our findings suggest that IL33 may exert its anti-fibrotic effects, at least in part, by modulating this pathway. Future studies will further investigate the direct mechanistic interactions between IL33, JMJD3, and TGF-β signaling in endometrial fibrosis. The activation of the ST2-JMJD3 axis is essential for LPMs-derived IL33 to exert its inhibitory effect on endometrial fibrosis. Regarding the regulation of IL33 expression, we discovered that the Lars-Fos axis plays a pivotal role. Lars, known to activate the mTOR signaling pathway via mTORC1 activation [40], was identified as a key regulator in this process. The mTOR pathway can modulate the expression of Fos [41]. For the first time, we reported that Lars upregulated IL33 expression in activated LPMs by regulating Fos, which binds to the enhancer region of the *Il33* gene.

The rapid migration of LPMs to the injured endometrium (peaking at 6 h post-injury) suggests that early interventions targeting LPMs recruitment could prevent fibrosis progression. For example, local administration of LPMs or their secreted IL33, potentially via an intrauterine hydrogel delivery system, may promote endometrial repair in patients. Furthermore, the observed correlation between IL33 levels in endometrial LPMs and IUA disease severity suggests that IL33 could serve as a dynamic biomarker for monitoring disease progression and treatment response in IUA patients. Further validation in clinical samples would be necessary to assess its diagnostic and prognostic potential. However, our mouse model does not fully recapitulate the pathophysiology of human IUA, particularly the chronic inflammation induced by repeated injuries. The role of IL33 in human endometrium remains controversial. Some studies have reported a pro-fibrotic effect of IL33 via fibroblast activation, which contrasts with our anti-fibrotic findings. Our findings highlight the dose-dependent dual roles of IL-33, where controlled low-dose administration exerts anti-fibrotic effects through ST2-JMJD3 activation, while previous studies suggest that high-dose IL-33 may promote fibrosis via excessive type 2 immune responses. This discrepancy may arise from differences in tissue-specific microenvironments or IL33-producing cell populations. Although our data highlight the therapeutic potential of IL33 in endometrial fibrosis, its systemic application may lead to off-target effects, especially in non-target organs where IL33 could exert pro-fibrotic or immune-activating functions. Future studies focusing on localized delivery systems or LPM-targeted approaches are essential to ensure efficacy and safety in clinical translation.

The endometrium stands unique among mammalian tissues, possessing the remarkable capacity for complete functional regeneration after cyclical shedding. Under physiological conditions, the endometrium undergoes a series of proliferation, differentiation, and shedding phases, allowing for full functional repair without the formation of scar tissue [42]. Endometrial damage incurred during surgical procedures, such as curettage, shares similarities with natural endometrial shedding during menstruation [4,43]. In both scenarios, the endometrial lining is shed, leading to cell death and the release of tissue fragments, which in turn release

Fig. 6. Lars-Fos axis upregulates *Il33* expression in LPMs by modulating enhancers. A. KEGG enrichment analysis of all differentially up-expressed genes in 6 h in LPMs after AES treated. B. GO enrichment analysis of all differentially up-expressed genes in 6 h in LPMs after AES treated. C. GSEA enrichment analysis of all differentially up-expressed genes in 6 h in LPMs after AES treated. D. The thermogram of AMINOACYL TRNA LIGASEACTIVITY pathway related genes expression pattern. E. The gene levels of *Lars* were detected with qRT-PCR (n = 5–6). F. Interaction plot of TOP 10 transcription factors associated with up-regulation DEGs (ChEA3: <https://maayanlab.cloud/chEA3/>). G. The gene levels of *Fos* were detected with qRT-PCR (n = 6). H. Protein interactions between *Lars* and up-regulation DEGs-associated TOP10 transcription factors (String: <https://cn.string-db.org/>). I. The gene levels of *Lars* and *Fos* were detected with qRT-PCR (n = 5–6). J. The gene levels of *Il33* were detected with qRT-PCR (n = 5). K. The protein levels of *Il33* were detected with immunofluorescence (n = 3, scale bar = 40 µm). L. Schematic diagram of plasmid construction. M. Dual luciferase reporter assay demonstrated that *Fos* positively regulates *Il33* expression by binding to enhancers (n = 3). (F-P-WT: co-transfection of *fos* plasmid with promoter plasmid. F-P-MUT: co-transfection of *fos* plasmid with mutant promoter plasmid. F-E-WT: co-transfection of *fos* plasmid with enhancer plasmid. F-E-MUT: co-transfection of *fos* plasmid with mutant enhancer plasmid.). Values are mean ± SD. *p < 0.05, **p < 0.01, ***p < 0.001, ****p < 0.0001, ns denotes p > 0.05 (by unpaired Student's t test or one-way ANOVA).

DAMPs, triggering a state of sterile inflammation [44]. In a mouse model mimicking menstruation, we found that LPMs migrated from the peritoneal cavity to the uterus during endometrial shedding induced by hormone withdrawal (Supplementary Fig. 8). Building upon this finding and our previous research, we propose that this migration of LPMs may contribute to the physiological, scar-free repair of the endometrium that is characteristic of menstruation in mammals.

However, our study has some limitations. The unique anatomical position of the uterus limited the effectiveness of current fluorescent cell-tracking probes, preventing direct visualization of LPMs migration to the endometrium. While photoconversion could be a potential solution, the uterus's deep location poses challenges for light penetration, requiring specialized optical setups to ensure sufficient labeling of abdominal cells. Although peritoneal lavage is not exclusively specific to LPMs, our approach preserved SPMs while reducing LPMs, offering better selectivity than clodronate liposomes. Furthermore, the observed redistribution of CD45.1⁺ LPMs from the peritoneal cavity to the uterus upon injury suggests active recruitment to the damaged tissue, despite the possibility of partial attachment to the uterine surface. Additionally, generating myeloid-specific GATA6 and IL33 double-knockout mice, which would provide stronger evidence, was constrained by the lengthy breeding cycles required. Future studies will focus on developing advanced live-cell tracking techniques and utilizing genetically engineered models to further validate and expand on these findings. We also recognize that our clinical sample size is relatively small. Future studies will aim to expand the sample size across different IUA severity levels to further investigate the correlation between IL33 expression and disease progression. Moreover, while the mouse model provides valuable mechanistic insights, it does not fully replicate human IUA pathophysiology, particularly due to the absence of a physiological hormonal cycle in mice. To address this, further validation in non-human primates or human endometria. This biopsy samples would be beneficial for tracking LPMs migration and IL33 secretion in a physiologically relevant setting.

While our study identifies LPMs as key players in endometrial repair, emerging evidence suggests that crosstalk between macrophage subsets may orchestrate tissue regeneration. Previous studies, including our own research on CD301⁺ and CX3CR1⁺ macrophages in IUA, indicate that additional macrophage subsets may contribute to the repair process, potentially through cooperative interactions. Future studies will employ spatial transcriptomics and lineage-tracing approaches to explore the functional interplay among macrophage subsets during endometrial regeneration. In addition, targeting the Lars-Fos axis represents a promising therapeutic strategy for fibrotic diseases, as it plays a role in IL33 regulation and macrophage-mediated fibrosis inhibition. Further investigation into pharmacological modulators of Lars-Fos signaling may provide new insights into developing targeted therapies for IUA and other fibrotic disorders.

In conclusion, our study revealed that DAMPs released by mechanically injured ESCs stimulate the migration of LPMs to the damaged uterus. These LPMs then upregulate IL33 expression via the Lars-Fos axis, achieved through binding to the enhancer region of the *IL33* gene. LPMs-derived IL33 inhibits the differentiation of ESCs into myofibroblasts by binding to ST2 receptor on the surface of ESCs. This interaction subsequently upregulates JMJD3 expression and suppresses fibrotic transformation, thereby preventing endometrial fibrosis and alleviating the severity of endometrial injury. Our findings underscore the pivotal role of LPMs in endometrial repair, with LPMs-derived IL33 playing a central role in maintaining endometrial homeostasis and preventing pathological fibrosis.

Compliance with ethics requirements

This study was approved by the Ethics Committee of the Affiliated Drum Tower Hospital of Nanjing University (No. 2021-078-01) and all participants have provided informed consent before the endometrial biopsy. For animal experiments, all experiments involving animals were conducted according to the ethical policies and procedures approved by the Animal Protection and Ethics Committee of Nanjing University (IACUC-D2202077) followed the guidelines of the National Institutes of Health (NIH) for the care and use of laboratory animals. Every effort was made to minimize animal suffering and the number of animals used in the experiments.

The authors declare that they have adhered to the ethical standards required for conducting research with human and animal subjects and have no conflicts of interest to disclose.

Declaration of competing interest

The authors declare that they have no known competing financial interests or personal relationships that could have appeared to influence the work reported in this paper.

Acknowledgements

We thank Yang Cheng (Cornell University, Department of Molecular Biology and Genetics) for her assistance and technical expertise. This work was supported by National Key R&D Program of China (2021YFC2701603), National Natural Science Foundation of China (82471663, 82271653, 82071600), Jiangsu Provincial Obstetrics and Gynecology Innovation Center (CXZX202229) and Jiangsu Biobank of Clinical Resources (BM2015004).

Appendix A. Supplementary material

Supplementary data to this article can be found online at <https://doi.org/10.1016/j.jare.2025.06.088>.

References

- [1] Ang CJ, Skokan TD, McKinley KL. Mechanisms of regeneration and fibrosis in the endometrium. *Annu Rev Cell Dev Biol* 2023;39(1):197–221. doi: <https://doi.org/10.1146/annurev-cellbio-011723-021442>.
- [2] Salamonson LA, Hutchison JC, Gargett CE. Cyclical endometrial repair and regeneration. *Development* 2021;148:17. doi: <https://doi.org/10.1242/dev.199577>.
- [3] Buechler MB, Kim KW, Onufer EJ, Williams JW, Little CC, Dominguez CX, et al. A stromal niche defined by expression of the transcription factor WT1 mediates programming and homeostasis of cavity-resident macrophages. *Immunity* 2019;51(1):119–130 e5. doi: <https://doi.org/10.1016/j.immuni.2019.05.010>.
- [4] Evans J, Salamonson LA. Inflammation, leukocytes and menstruation. *Rev Endocr Metab Disord* 2012;13(4):277–88. doi: <https://doi.org/10.1007/s11154-012-9223-7>.
- [5] The American Fertility Society classifications of adnexal adhesions, distal tubal occlusion, tubal occlusion secondary to tubal ligation, tubal pregnancies, mullerian anomalies and intrauterine adhesions. *Fertil Steril* 1988;49(6): p. 944–55. doi: [10.1016/s0015-0282\(16\)59942-7](https://doi.org/10.1016/s0015-0282(16)59942-7).
- [6] Deans R, Vancailie T, Ledger W, Liu J, Abbott JA. Live birth rate and obstetric complications following the hysteroscopic management of intrauterine adhesions including Asherman syndrome. *Hum Reprod* 2018;33(10):1847–53. doi: <https://doi.org/10.1093/humrep/dev237>.
- [7] Chen Y, Liu L, Luo Y, Chen M, Huan Y, Fang R. Prevalence and impact of chronic endometritis in patients with intrauterine adhesions: a prospective cohort study. *J Minim Invasive Gynecol* 2017;24(1):74–9. doi: <https://doi.org/10.1016/j.jmig.2016.09.022>.
- [8] Sun H, Dong J, Fu Z, Lu X, Chen X, Lei H, et al. TSG6-Exo/CS/GP attenuates endometrium fibrosis by inhibiting macrophage activation in a murine IUA model. *Adv Mater* 2024;36(21):e2308921. doi: <https://doi.org/10.1002/adma.202308921>.
- [9] Liu D, Wang J, Zhao G, Jiang P, Song M, Ding H, et al. CSF1-associated decrease in endometrial macrophages may contribute to Asherman's syndrome. *Am J Reprod Immunol* 2020;83(1):e13191. doi: <https://doi.org/10.1111/aji.13191>.

- [10] Liang Y, Meng J, Yu Z, Guo Y, Zhang X, Yan Y, et al. Ru single-atom nanozymes targeting ROS-ferroptosis pathways for enhanced endometrial regeneration in intrauterine adhesion therapy. *Biomaterials* 2025;315:122923. doi: <https://doi.org/10.1016/j.biomaterials.2024.122923>.
- [11] Lv H, Sun H, Wang L, Yao S, Liu D, Zhang X, et al. Targeting CD301(+) macrophages inhibits endometrial fibrosis and improves pregnancy outcome. *EMBO Mol Med* 2023;15(9):e17601. doi: <https://doi.org/10.15252/emmm.202317601>.
- [12] Wang J, Li D, Pan Y, Li J, Jiang Q, Liu D, et al. Interleukin-34 accelerates intrauterine adhesions progress related to CX3CR1(+) monocytes/macrophages. *Eur J Immunol* 2021;51(10):2501–12. doi: <https://doi.org/10.1002/eji.202149174>.
- [13] Sun K, Li YY, Jin J. A double-edged sword of immuno-microenvironment in cardiac homeostasis and injury repair. *Signal Transduct Target Ther* 2021;6(1):79. doi: <https://doi.org/10.1038/s41392-020-00455-6>.
- [14] Simkin J, Aloysius A, Adam M, Safaei F, Donahue RR, Biswas S, et al. Tissue-resident macrophages specifically express Lactotransferrin and Vegf during ear pinna regeneration in spiny mice. *Dev Cell* 2024;59(4):496–516 e6. doi: <https://doi.org/10.1016/j.devcel.2023.12.017>.
- [15] Honda M, Kadohisa M, Yoshii D, Komohara Y, Hibi T. Directly recruited GATA6 + peritoneal cavity macrophages contribute to the repair of intestinal serosal injury. *Nat Commun* 2021;12(1). doi: <https://doi.org/10.1038/s41467-021-27614-9>.
- [16] Wang J, Kubes P. A reservoir of mature cavity macrophages that can rapidly invade visceral organs to affect tissue repair. *Cell* 2016;165(3):668–78. doi: <https://doi.org/10.1016/j.cell.2016.03.009>.
- [17] Lv H, Nan Z, Jiang P, Wang Z, Song M, Ding H, et al. Vascular endothelial growth factor 165 inhibits pro-fibrotic differentiation of stromal cells via the DLL4/Notch4/smad7 pathway. *Cell Death Dis* 2019;10(9):681. doi: <https://doi.org/10.1038/s41419-019-1928-z>.
- [18] Wang J, Li J, Yin L, Wang X, Dong Y, Zhao G, et al. MSCs promote the efferocytosis of large peritoneal macrophages to eliminate ferroptotic monocytes/macrophages in the injured endometria. *Stem Cell Res Ther* 2024;15(1):127. doi: <https://doi.org/10.1186/s13287-024-03742-z>.
- [19] Li J, Pan Y, Yang J, Wang J, Jiang Q, Dou H, et al. Tumor necrosis factor- α -primed mesenchymal stem cell-derived exosomes promote M2 macrophage polarization via Galectin-1 and modify intrauterine adhesion on a novel murine model. *Front Immunol* 2022;13:945234. doi: <https://doi.org/10.3389/fimmu.2022.945234>.
- [20] Yin L, Bing Z, Zheng Y, Pan Y, Dong Y, Wang J, et al. Oroxylin A-induced trained immunity promotes LC3-associated phagocytosis in macrophage in protecting mice against sepsis. *Inflammation* 2024. doi: <https://doi.org/10.1007/s10753-024-02033-2>.
- [21] Deniset JF, Belke D, Lee WY, Jorch SK, Deppermann C, Hassanabad AF, et al. Gata6(+) pericardial cavity macrophages relocate to the injured heart and prevent cardiac fibrosis. *Immunity* 2019;51(1):131–140 e5. doi: <https://doi.org/10.1016/j.immuni.2019.06.010>.
- [22] Louwe PA, Badiola Gomez L, Webster H, Perona-Wright G, Bain CC, Forbes SJ, et al. Recruited macrophages that colonize the post-inflammatory peritoneal niche convert into functionally divergent resident cells. *Nat Commun* 2021;12(1):1770. doi: <https://doi.org/10.1038/s41467-021-21778-0>.
- [23] Li C, Cai C, Xu D, Chen X, Song J. TREM1: Activation, signaling, cancer and therapy. *Pharmacol Res* 2024;204:107212. doi: <https://doi.org/10.1016/j.phrs.2024.107212>.
- [24] Zhao Y, Guo Y, Jiang Y, Pan Y, Zhu X, Zhang X. Vitamin D suppresses macrophage infiltration by down-regulation of TREM-1 in diabetic nephropathy rats. *Mol Cell Endocrinol* 2018;473:44–52. doi: <https://doi.org/10.1016/j.mce.2018.01.001>.
- [25] Pakshir P, Noskovicova N, Lodyga M, Son DO, Schuster R, Goodwin A, et al. The myofibroblast at a glance. *J Cell Sci* 2020;133(13). doi: <https://doi.org/10.1242/jcs.227900>.
- [26] Yu C, Xiong C, Tang J, Hou X, Liu N, Bayliss G, et al. Histone demethylase JMJD3 protects against renal fibrosis by suppressing TGF β and Notch signaling and preserving PTEN expression. *Theranostics* 2021;11(6):2706–21. doi: <https://doi.org/10.7150/thno.48679>.
- [27] Kim S, Yoon I, Son J, Park J, Kim K, Lee JH, et al. Leucine-sensing mechanism of leucyl-tRNA synthetase 1 for mTORC1 activation. *Cell Rep* 2021;35(4):109031. doi: <https://doi.org/10.1016/j.celrep.2021.109031>.
- [28] Raphael HE, Hassan GF, Osorio OA, Cohen LS, Payne MD, Katz-Kiriakos E, et al. Activator protein transcription factors coordinate human IL-33 expression from noncanonical promoters in chronic airway disease. *JCI Insight* 2024;9(5). doi: <https://doi.org/10.1172/jci.insight.174786>.
- [29] Gosselin D, Link VM, Romanoski CE, Fonseca GJ, Eichenfield DZ, Spann NJ, et al. Environment drives selection and function of enhancers controlling tissue-specific macrophage identities. *Cell* 2014;159(6):1327–40. doi: <https://doi.org/10.1016/j.cell.2014.11.023>.
- [30] Zindel J, Peiseler M, Hossain M, Deppermann C, Lee WY, Haenni B, et al. Primordial GATA6 macrophages function as extravascular platelets in sterile injury. *Science* 2021;371(6533). doi: <https://doi.org/10.1126/science.abe0595>.
- [31] Chen W-Y, Wu Y-H, Tsai T-H, Li R-F, Lai A-C-Y, Li L-C, et al. Group 2 innate lymphoid cells contribute to IL-33-mediated alleviation of cardiac fibrosis. *Theranostics* 2021;11(6):2594–611. doi: <https://doi.org/10.7150/thno.51648>.
- [32] Nagashima R, Ishikawa H, Kuno Y, Kohda C, Iyoda M. IL-33 attenuates renal fibrosis via group2 innate lymphoid cells. *Cytokine* 2022;157:155963. doi: <https://doi.org/10.1016/j.cyto.2022.155963>.
- [33] He R, Yin H, Yuan B, Liu T, Luo L, Huang P, et al. IL-33 improves wound healing through enhanced M2 macrophage polarization in diabetic mice. *Mol Immunol* 2017;90:42–9. doi: <https://doi.org/10.1016/j.molimm.2017.06.249>.
- [34] Schiering C, Krausgruber T, Chomka A, Fröhlich A, Adelman K, Wohlfert EA, et al. The alarmin IL-33 promotes regulatory T-cell function in the intestine. *Nature* 2014;513(7519):564–8. doi: <https://doi.org/10.1038/nature13577>.
- [35] Gao Y, Luo C, Rui T, Fan Y, Yao Y, Shen H, et al. Autophagy inhibition facilitates wound closure partially dependent on the YAP/IL-33 signaling in a mouse model of skin wound healing. *FASEB J* 2021;35(10). doi: <https://doi.org/10.1096/fj.202002623RRR>.
- [36] Liu D, Yuan L, Xu F, Ma Y, Zhang H, Jin Y, et al. Interleukin-33 promotes intrauterine adhesion formation in mice through the mitogen-activated protein kinase signaling pathway. *Commun Biol* 2024;7(1). doi: <https://doi.org/10.1038/s42003-024-06709-1>.
- [37] Tan Z, Liu Q, Jiang R, Lv L, Shoto SS, Maillet I, et al. Interleukin-33 drives hepatic fibrosis through activation of hepatic stellate cells. *Cell Mol Immunol* 2017;15(4):388–98. doi: <https://doi.org/10.1038/cmi.2016.63>.
- [38] Rankin AL, Mumm JB, Murphy E, Turner S, Yu N, McClanahan TK, et al. IL-33 induces IL-13-dependent cutaneous fibrosis. *J Immunol* 2010;184(3):1526–35. doi: <https://doi.org/10.4049/jimmunol.0903306>.
- [39] Salm L, Shim R, Noskovicova N, Kubes P. Gata6(+) large peritoneal macrophages: an evolutionarily conserved sentinel and effector system for infection and injury. *Trends Immunol* 2023;44(2):129–45. doi: <https://doi.org/10.1016/j.it.2022.12.002>.
- [40] Kim K, Yoo HC, Kim BG, Kim S, Sung Y, Yoon I, et al. O-GlcNAc modification of leucyl-tRNA synthetase 1 integrates leucine and glucose availability to regulate mTORC1 and the metabolic fate of leucine. *Nat Commun* 2022;13(1):2904. doi: <https://doi.org/10.1038/s41467-022-30696-8>.
- [41] Jiang W, Rixiati Y, Huang H, Shi Y, Huang C, Jiao B. Asperolide A prevents bone metastatic breast cancer via the PI3K/AKT/mTOR/c-Fos/NFATc1 signaling pathway. *Cancer Med* 2020;9(21):8173–85. doi: <https://doi.org/10.1002/cam4.3432>.
- [42] Evans J, Salamonsen LA, Winship A, Menkhurst E, Nie G, Gargett CE, et al. Fertile ground: human endometrial programming and lessons in health and disease. *Nat Rev Endocrinol* 2016;12(11):654–67. doi: <https://doi.org/10.1038/nrendo.2016.116>.
- [43] Maybin JA, Critchley HO. Menstrual physiology: implications for endometrial pathology and beyond. *Hum Reprod Update* 2015;21(6):748–61. doi: <https://doi.org/10.1093/humupd/dmv038>.
- [44] Gong T, Liu L, Jiang W, Zhou R. DAMP-sensing receptors in sterile inflammation and inflammatory diseases. *Nat Rev Immunol* 2019;20(2):95–112. doi: <https://doi.org/10.1038/s41577-019-0215-7>.